HELMHOLTZ INSTITUTE FREIBERG
FOR RESOURCE TECHNOLOGY

Freiberg, 08/07/2024

Optimierte Prozessketten für hydromechanisches Li-Ionen-Batterie-Recycling Helmholtz-Institut Freiberg für Ressourcentechnologie (HIF)

1. Project Overview

ZE: Helmholtz-Zentrum Dresden-Rossendorf (HZDR), Helmholtz-Institut Freiberg für Ressourcentechnologie (HIF)
Förderkennzeichen: 03XP0339B
Laufzeit des Vorhabens: 2023-2024
Berichtszeitraum: 2023-2024
Vorhabenbezeichnung: Optimierte Prozessketten für hydromechanisches Li-Ionen-Batterie-Recycling – HydroLIBRec.
Leitung: AP 6. Prozesssimulation der technisch-physikalischen Aspekte der Recyclingverfahren (Energieströme, Materialeigenschaften, Prozessparameter). AP8. Ableitung von Design-for-Recycling-Konzepten auf Material- bis Zellebene.

List of Figures

List of Tables

Contents

2. Summary

The study aimed to develop design for recycling (DfR) recommendations for NMC 811 batteries using a well-defined recycling process. The methodology integrated comprehensive empirical and analytical measurements to construct an accurate thermodynamic simulation of material and substance flow throughout the recycling process. This involved stages of manual dismantling, followed by mechanical, physical, and metallurgical processing of the NMC 811 battery cells. Thermodynamic simulations were conducted using FactSage™ version 8.2 and HSC Chemistry 10 version 10.3.7.1 software to model the recovery of lithium present in the black mass via metallurgical processing methods. The results provided a detailed breakdown of the material composition post-dismantling, revealing that separated cells containing the active NMC 811 material constituted 63.7% of the total weight. The study also introduced a recyclability index to quantify the recovery rates of individual elements, showcasing a recovery rate of 59.7% for lithium and an overall recycling index of 59.4%. The generated data was meticulously formatted to ensure clear comprehension, thereby supporting informed decision-making for optimizing recycling strategies. Key conclusions emphasized the importance of integrating comprehensive material flow analysis and adopting a product-centric approach to enhance recycling efficiency. Recommendations included optimizing the dismantling process to achieve a 21% reduction in environmental impacts, such as Global Warming Potential, and avoiding the use of materials that would be lost in the recycling route. These measures are projected to increase the recycling index to 90%, thereby significantly improving the overall sustainability of the recycling process for NMC 811 batteries.

3. Report Overview

The first step in optimizing the hydromechanical Li-ion battery recycling system simulation involves a comprehensive analysis of material and substance flow, emphasizing the characteristics and composition of the recyclates, labeled as AP6. As shown in Figure 1, the outlined block flow diagram encompasses pretreatment procedures, notably the manual dismantling of NMC 811 battery cells from the 18650 series, followed by mechanical, physical, and metallurgical processing units.

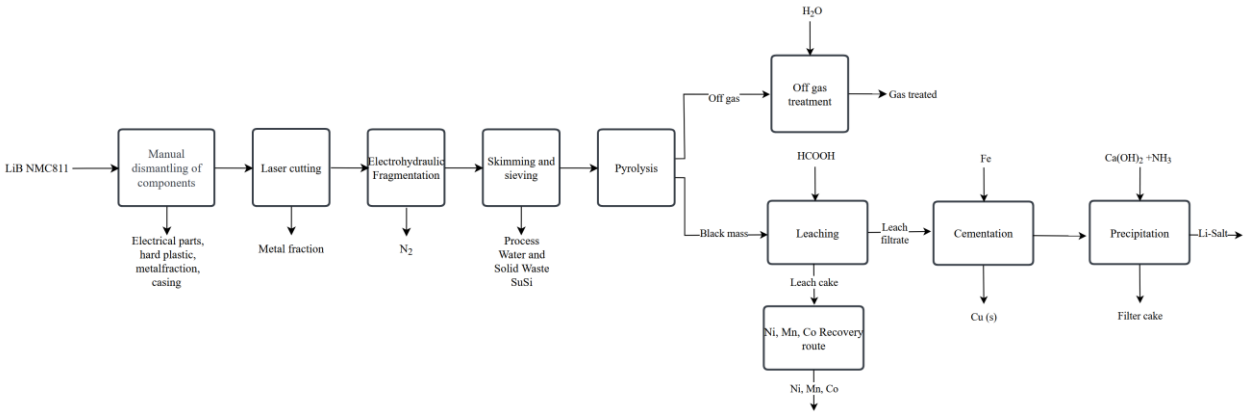

Figure 1. Block flow diagram of recycling process of Li-salt from Li-ion battery NMC811.

Continuing along the recycling route, as illustrated in Figure 2, a physical processing unit is utilized, employing a laser cut on the battery cell to facilitate the detachment of the casing, thereby improving the liberation of materials within the cells. Following this step, the Electrohydraulic Fragmentation (EHZ) method is applied, followed by the skim and sieve (SuSi) process unit.

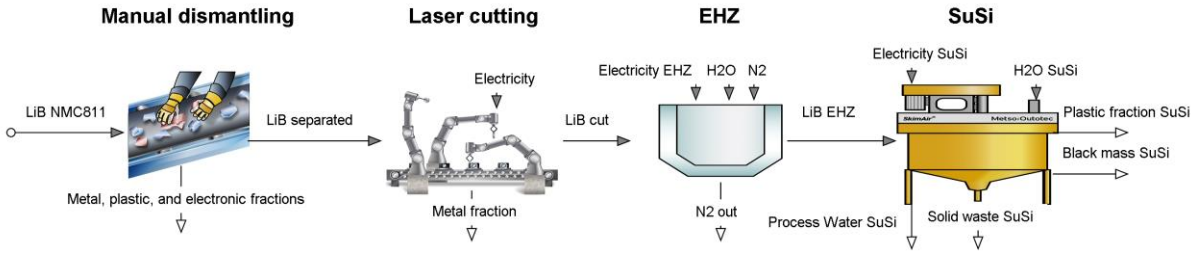

Figure 2. HSC Simulation Flowsheet for the manual dismantling, mechanical, and physical recycling processes involved in extracting Li-salt from NMC811 lithium-ion batteries.

The intermediate product, known as Black Mass SuSi, obtained after the SuSi process unit, undergoes pyrolysis as shown in Figure 3. The resulting black mass is then processed through leaching, cementation, and precipitation using respective hydrometallurgical methods to produce Li-salt as the final product. The development of the thermodynamic-based simulation model utilized HSC Chemistry 10 version 10.3.7.1 and FactSageTM version 8.2. Insights from this simulation are essential for applying the DfR Principles, as outlined in AP8.

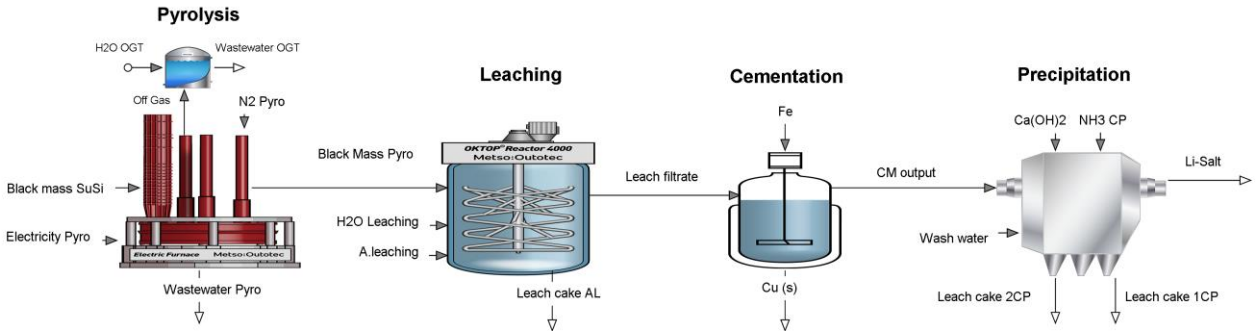

Figure 3. HSC Simulation Flowsheet for the metallurgical processing method, encompassing both pyrometallurgical and hydrometallurgical units, utilized in the extraction of Li-salt from NMC811 lithium-ion batteries.

4. Methodology

For the thermodynamic simulation, accurate material flow and elemental composition are essential. This requires data from both empirical measurements, provided by FactSage, and analytical measurements such as Inductively Coupled Plasma - Optical Emission Xmetry (ICP-OES) and X-Ray Diffraction (XRD) analysis. Consequently, the composition of the material undergoing metallurgical processing will be as precise as possible. As

shown in Figure 4, a material flow analysis detailing the weight of each process unit was created. Additionally, Table 1 presents the weight percentage composition following manual dismantling, sourced from IWKS. This data provides a detailed breakdown of components obtained from the manual dismantling of NMC 811 Li-ion batteries, which is crucial for understanding material distribution and potential recovery. Among these components, the separated cells constitute the largest share at 63.7%, primarily containing the active NMC 811 material. This fraction will be the only one considered for the hydromechanical Li-ion battery recycling system simulation. Additionally, hard plastic and rubber insulation account for 14.8%, while the plastic cover represents a minor component at 0.6%. The metal fraction comprises 2.5%, potentially including small metallic parts suitable for separate recycling routes. The aluminum casing is a significant material, making up 17.2% of the total. Electronics represent the smallest fraction at 1.2%, which may include valuable metals for further recycling processes such as gold, silver, and palladium.

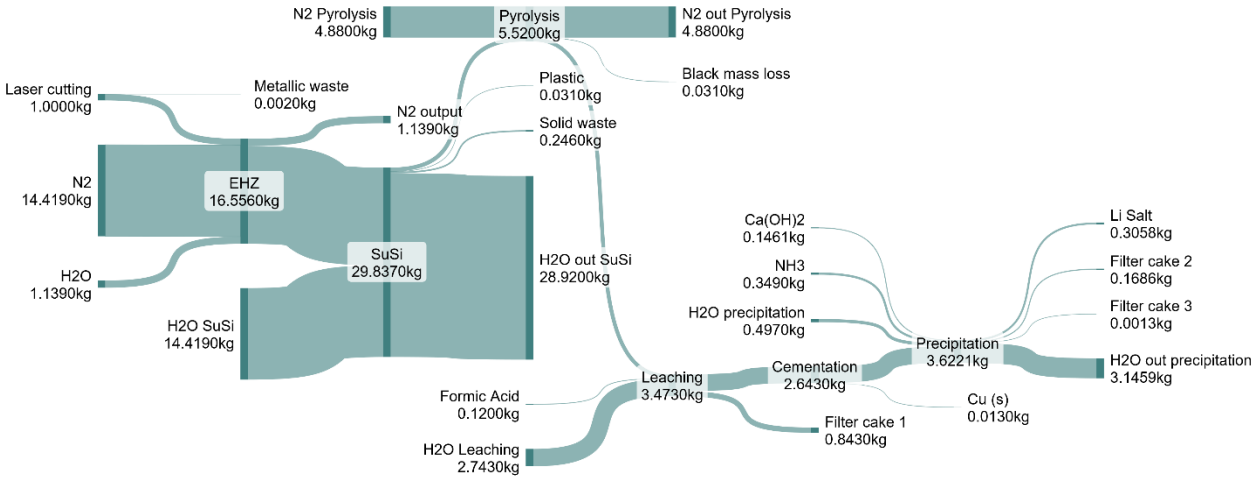

Figure 4. Material flow analysis detailing the weight of each process until the extraction of Li-salt from NMC811 lithium-ion batteries.

Table 1. Composition (in wt.- %) of 40 cells NMC811 expended battery.

Manual Dismantling			
NMC811	Material	kg	wt.- %
40 cells	Separated Cells	1.84776	63.7
	Hard Plastic: Rubber, Insulation, Lid or Cover, Fastenings or Fixations, minimal contamination with metal/cables	0.42912	14.8
	Plastic Cover	0.01733	0.6
	Metal fraction	0.07318	2.5
	Casing (Aluminum)	0.5	17.2

Electronics	0.03418	1.2
Total	2.90	100

4.1. Laser cutting

The separate cell, acquired post-manual dismantling, required thorough characterization of its elemental composition, encompassing the anode, cathode, casing, and electrolyte components within the battery cell, quantified in both mass and weight percentage. Subsequently, the laser-cutting process was conducted at Frauenhofer IWKS with the objective of facilitating the detachment and liberation of the casing of the NMC811 battery cell. The laser cutting procedure was executed twice to enhance the liberation efficiency. As demonstrated in Table 2, the only losses incurred were observed in the casing material, notably with regards to Fe and Ni.

Table 2. Elemental Composition (in wt.-%) of spent NMC811 battery and material flow post-laser cutting process unit.

Input Laser 2 Cut - Separated Cell 1 kg				**Output Laser Cut**	
Cell Component	**Composition**	**[wt%]**	**Kg**	**Kg**	**[wt%]**
Anode	Cu	7.000	0.070	0.070	7.014
Anode	C	25.400	0.254	0.254	25.451
Cathode	Al	4.970	0.050	0.050	4.980
Cathode-Active Material NMC 811	Li	2.504	0.025	0.025	2.509
	Ni	16.941	0.169	0.169	16.975
	Mn	1.982	0.020	0.020	1.986
	Co	2.126	0.021	0.021	2.131
	O	11.546	0.115	0.115	11.569
Anode Binder PVDF fluoropolymer	C2H2F2	3.000	0.030	0.030	3.006
Case-Steel	Fe	5.616	0.056	0.055	5.527
	Ni	3.024	0.030	0.029	2.930
Separator foil	C2H4	1.850	0.019	0.019	1.854
Elektrolyt, org. Carbonate	LiPF6	2.808	0.028	0.028	2.814
	C3H4O3	2.808	0.028	0.028	2.814
	C4H6O3	2.808	0.028	0.028	2.814
	C3H6O3	2.808	0.028	0.028	2.814
	C5H10O3	2.808	0.028	0.028	2.814
Total		100	1	0.998	100

4.2. Electrohydraulic fragmentation

EHZ conducted at Fraunhofer IWKS utilizes medium-voltage electrical discharges in a liquid medium (H2O), supplemented with N2 to mitigate side reactions. This procedure is designed to fragment or break down materials found in the spent NMC 811 battery cell. The intense electrical discharges induce shock waves within the medium, resulting in the mechanical fragmentation of the material. This prepares the material for subsequent processing units. Importantly. As shown in Table 3, no losses have been detected in for material flow analysis during this process.

Table 3. Input material considered for the EHZ process unit.

Input EHZ			
Cell Component	**Composition**	**Kg**	**[wt%]**
Anode	Cu	0.070	6.98
Anode	C	0.254	25.31
Cathode	Al	0.050	4.95
Cathode-Active Material NMC 811	Li	0.025	2.50
	Ni	0.169	16.88
	Mn	0.020	1.98
	Co	0.021	2.12
	O	0.115	11.51
Cathode Binder PVDF fluoropolymer	C2H2F2	0.030	2.99
Case-Steel	Fe	0.055	5.50
	Ni	0.029	2.91
Extra-Element in Off-Gas and Black Mass	B	0.0001	0.01
	S	0.001	0.06
	Ca	0.001	0.13
	Mg	0.0002	0.02
	Na	0.00004	0.00
	Si	0.003	0.32
Separator foil	C2H4	0.019	1.84
Elektrolyt, org. Carbonate	LiPF6	0.028	2.80
	C3H4O3	0.028	2.80
	C4H6O3	0.028	2.80
	C3H6O3	0.028	2.80
	C5H10O3	0.028	2.80
Total		1.00	100
Water	H20	14.41	
N2	N2	1.14	
Total		16.556	

4.3. Skim and Sieve

Following the EHZ process unit, the intermediate product undergoes further refinement through the SuSi process, conducted at IME Fraunhofer. This process is meticulously designed to segregate materials based on their size and density, thereby enhancing the liberation of the intermediate product. Within this unit, medium electricity voltage and water are employed in the mechanical separation process to achieve optimal results. As outlined in Table 4, losses can be quantified in graphite from the anode, as well as in Fe and Ni from the casing material. Additionally, losses are noted in the separator foil and organic carbonates.

Table 4. Material flow in SuSi process.

		Input SuSi		Output SuSi	
Cell Component	**Composition**	**Kg**	**[wt%]**	**kg**	**[wt%]**
Anode	Cu	0.0700	6.975	0.070	10.938
Anode	C	0.2540	25.311	0.080	12.475
Cathode	Al	0.0497	4.952	0.050	7.765
Cathode-Active Material NMC 811	Li	0.0250	2.495	0.025	3.913
	Ni	0.1694	16.882	0.169	26.471
	Mn	0.0198	1.975	0.020	3.097
	Co	0.0213	2.119	0.021	3.322
	O	0.1155	11.505	0.115	18.040
Cathode Binder PVDF fluoropolymer	C2H2F2	0.0300	2.989	0.030	4.688
Case-Steel	Fe	0.0552	5.497	0.017	2.625
	Ni	0.0292	2.914	0.009	1.416
Extra-Element in Off-Gas and Black Mass	B	0.0001	0.011	0.0001	0.017
	S	0.0006	0.062	0.0006	0.097
	Ca	0.0013	0.128	0.0013	0.201
	Mg	0.0002	0.024	0.0002	0.037
	Na	0.00004	0.004	0.00004	0.006
	Si	0.0032	0.321	0.003	0.504
Separator foil	C2H4	0.018	1.844		
Elektrolyt, org. Carbonate	LiPF6	0.028	2.79	0.0281	4.387
	C3H4O3	0.028	2.79		
	C4H6O3	0.028	2.79		
	C3H6O3	0.028	2.79		
	C5H10O3	0.028	2.79		
Total		1.00	100	0.64	100
Water	H20 mixed	14.41			
Total		15.41			
Water	H2O	14.41			
Total		29.83			

4.4. Pyrolysis

Pyrolysis is a key component of the recycling process for NMC 811 expended batteries due to its ability to thermally decompose organic constituents in the absence of oxygen. Specifically, in the context of recycling, pyrolysis facilitates the disassembly of the battery's complex structure, effectively segregating organic materials from inorganic components. This procedure, conducted at IME Fraunhofer at a temperature of 500°C, utilizes medium voltage electricity and N_2 to maintain an inert environment. It involves comprehensive analysis of both input and output products through techniques such as ICP-OES, shown in Table 5 and XRD analysis shown in Table 6. Additionally, the process is simulated using FactSage, providing empirical data shown in Table 7 for comparative analysis. The aim of this comparative analysis is to elucidate the composition of various phases present in the resulting black mass post-pyrolysis, which will undergo subsequent leaching. For instance, as indicated in Table 8, copper, initially present at 0.070 kg or 10.94%, undergoes transformations into different states such as Cu (0.067 kg, 10.98%), Cu4O3 (0.003 kg, 0.4%) and Cu2S (0.001 kg, 0.1%). Similarly, nickel transitions from 0.169 kg or 26.47% to 0.18 kg or 31.05%, accompanied by the formation of additional nickel oxide (NiO). Lithium undergoes transformations into compounds such as Li2CO3 (0.021 kg, 3.5%) and LiF (0.038 kg, 6.23%), among others. Notably, this process results in a reduction in total mass from 0.640 kg to 0.609 kg in the black mass output, reflecting the efficiency of material recovery and transformation, with the remaining mass accounted for as off-gas, and losses measured at 4.911 kg.

Table 5. ICP-OES analysis conducted by IME Fraunhofer post-pyrolysis (wt%).

Element	Wt %
Al	2.581
B	0.011
Ca	0.129
Co	3.922
Cu	3.674
Fe	1.453
Li	3.719
Mg	0.024
Mn	1.42
Na	0.004
Ni	32.633
P	0
S	0.062
Si	0.323
Insoluble	36.339
Total	86.293

Table 6. XRD Analysis by IME Fraunhofer Post-Pyrolysis (wt%).

Composition	wt%
Lithium Nickel Manganese Cobalt Oxide (Li1Ni0.75Mn0.1Co0.15O2)	27
Copper (Cu)	3
Zabuyelite (Li2CO3)	8
Paramelaconite (Cu4O3)	1
Nickel Oxide (NiO)	6
Nickel (Ni)	7
Graphite 3R (C)	48
Total	**100**

Table 7. Empirical data in (wt%) obtained through FactSage.

Al	Al2O3	B	C	C_graphite
3.12E-23	0.001622	2.16E-18	0.001191	0.235822138
Ca	**CaO**	**CaMg2Al16O27**	**CaF2**	**Co**
4.39E-25	3.01E-06	0.000354	0.001528	0.01222175
CoO	**Co_fcc**	**Cu**	**CuO**	**Cu_fcc**
0.000182	0.036272594	0.000163	1.50E-09	0.154382
Cu2S	**Fe**	**FeO**	**Fe2O3**	**Li**
0.005427	0.023262547	0.014927	0.000203632	2.45E-18
Li2O	**LiAlO2**	**LiF**	**LiAl5O8**	**Li3PO4**
1.38E-10	0.012674	0.031939	0.003037884	0.008803
Li2SiO3	**Mg**	**MgO**	**Mn**	**MnO**
0.003614549	9.04E-20	2.81E-05	8.29E-08	0.045247
Na	**Na2O**	**Na2Ca3Al16O28**	**Ni**	**NiO**
1.75E-25	1.85E-18	9.14E-05	0.027979	5.03E-06
Ni_fcc	**P**	**Si**		
0.37902	2.24E-15	6.03E-18		

Table 8. Material flow and metallurgical analysis of material transformations post-pyrolysis for NMC 811 expended battery.

Pyrolysis Input				Pyrolysis Output-Black Mass		
Cell Component	**Composition**	**kg**	**[wt%]**	**Composition**	**Kg**	**[wt%]**
Anode	Cu	0.070	10.94	Al2O3	0.049	8.15
Anode	C	0.080	12.47	B	0.00011	0.01
Cathode	Al	0.050	7.77	C	0.164	26.98

Cathode-Active Material NMC 811	Li	0.025	3.91	CaO	0.0009	0.14
	Ni	0.169	26.47	Co	0.015	2.50
	Mn	0.020	3.10	CoO	0.006	0.98
	Co	0.021	3.32	Cu	0.066	10.98
	O	0.115	18.04	Cu4O3	0.002	0.42
Anode Binder PVDF fluoropolymer	C2H2F2	0.030	4.69	Cu2S	0.0005	0.08
Case-Steel	Fe	0.017	2.62	Fe	0.012	2.08
	Ni	0.009	1.42	FeO	0.004	0.67
Extra-Element in Off-Gas and Black Mass	Br	0.0000001	0.00002	Li2CO3	0.021	3.49
	B	0.0001	0.02	LiF	0.037	6.22
	Cl	0.0000005	0.00008	Li2P04	0.005	0.93
	S	0.001	0.10	Li2SiO3	0.001	0.21
	Ca	0.001	0.20	MgO	0.0002	0.03
	Mg	0.0002	0.04	MnO	0.019	3.25
	Na	0.00004	0.01	Na2O	3.99E-05	0.006
	Si	0.003	0.50	Ni	0.189	31.04
Electrolyte, org. Carbonate	LiPF6	0.028	4.39	NiO	0.010	1.72
Total		0.640	100	**Total**	0.609	100
N2			4.88	Off-Gas	4.911	

4.5. Formic acid leaching

The initial hydrometallurgical processing phase of black mass recycling involves a leaching methodology operating at a temperature of 70°C, adhering to parameters provided by IME Fraunhofer. Within this methodology, a combination of formic acid, water, and electricity facilitates the alteration of the phases of valuable elements from the black mass. Through an interaction between the black mass and formic acid, chemical reactions are initiated, resulting in the formation of formate salts, including lithium formate, iron formate, and copper formate, as shown in table 9. In Table 10, the leaching yields obtained by IME Fraunhofer are presented. In this process, the precipitation of nickel, manganese, and cobalt in the filter cake requires hydrothermal treatment to facilitate their recovery and regeneration, thereby enabling their reuse as active cathode materials. This proposed process has not been simulated in this report; however, the hypothetical recovery has been considered.

Table 9. Aftermath of Hydrometallurgical Leaching Process Using Organic Formic Acid: Reactions and Products utilizing HSC Sim software.

Filtrate	**kg**	**wt%**
$Al(CHOO)_3$	0.014	0.005
$B(CHO2)_2$	0.0001	0.00004
C+H20	2.55	0.97
$Ca(CHO2)_2$	0.001	0.0003
$Co(CHO2)_2$	0.0002	0.0001
CoF	0.0002	0.0001
$Cu(CHO_2)_2$	0.013	0.005
$Fe(CHO_2)_2$	0.003	0.001
LiCHOO	0.041	0.015
$Mg(CHO_2)_2$	0.0002	0.0001
$Mn(CHO_2)_2$	0.002	0.001
$Ni(CHO_2)_2$	0.005	0.002
Total	**2.63**	**1**
Filter Cake	**kg**	**wt%**
Nickel Formate Hydrate Ni(HCOO)2(H2O)2	0.194	23.054
Cobalt Formate Hydrate Co(HCOO)2(H2O)2	0.021	2.473
C+H20	0.457	54.232
Manganese Hydroxide Oxide Mn(OH)O	0.018	2.107
Copper Formate Hydrate Cu(CHO2)2(H20)2	0.057	6.704
xAl2O3	0.036	4.261
FeO	0.014	1.655
Lithium Formate Hydrate Li(HCOO)2(H2O)2	0.026	3.041
Cobalt Oxide CoO	0.021	2.473
Total	**0.843**	**100**

Table 10. IME Fraunhofer's leaching yield data using formic acid.

Element	**Leaching yield %**
Al	27.72
Co	1.97
Cu	19.26
Fe	16.97
Li	61.31
Mn	10.39
Ni	2.66

4.6. Precipitation

After the leaching and before the precipitation phase, the cementation process unit is considered for copper recovery. However, due to the absence of experimental data for process parameters, this step was not simulated. Instead, and as shown in Table 11, the recovery of Cu was assumed based on the amount of copper in the leach filtrate as determined by the copper leaching yield.

Table 11. Cementation output product.

Filtrate	**kg**	**wt%**
Al(CHOO)3	0.0138	0.0052
B(CHO2)2	0.0001	0.00004
C+H2O	2.5502	0.9697
Ca(CHO2)2	0.0009	0.0003
Co(CHO2)2	0.0002	0.0001
CoF	0.0002	0.0001
Fe(CHO2)2	0.00001	0.00001
Cu(CHO2)2	0.0029	0.0011
Mn(CHO2)2	0.0406	0.0154
NaCHO2	0.0002	0.0001
Ni(CHO2)2	0.0021	0.0008
Total	2.63	1
Cementation Cake	**kg**	
Cu (s)	0.013	

Following cementation, the processed black mass proceeds to the precipitation phase, which involves two steps crucial for further isolating valuable elements. To facilitate precipitation reactions, calcium hydroxide (Ca(OH)2) is initially used for fluorine precipitation, followed by the introduction of ammonia (NH3) in a second step.

This stage initiates a series of chemical reactions that culminate in the formation of solid outputs, including waste and lithium salt. Table 12 details the sequence of reactions occurring during this step. The progress of the reactions was determined to achieve the values reported by IME Fraunhofer in the ICP-OES analysis of the lithium salt, as depicted in Table 13.

Table 12. Chemical balanced reactions for the precipitation process utilizing HSC Sim software.

Precipitation Output (Li Salt)		
Filtrate	**kg**	**wt%**
B(CHO2)2	0.00015	0.05
Ca(CHO2)2	0.18586	60.76
Co(CHO2)2	0.00003	0.01

Cu(CHO2)2	0.00001	0
Fe(CHO2)2	0.00014	0.05
LiCHOO	0.11780	38.51
Mg(CHO2)2	0.00002	0.01
Mn(CHO2)2	0.00005	0.02
NaCHO2	0.00087	0.29
Ni(CHO2)2	0.00019	0.06
Total	**0.3059**	**1**
(Calcium Hydroxide) Flouride Precipitation Output		
Precipitation Cake 1	**kg**	**wt%**
Al3(PO4)2(OH)3*5H2O	0.0048	2.83
MnAl2(PO4)2(OH)2*6H2O	0.0048	2.83
*3CaO*Al2O3*Ca(OH)2*18H2O	0.0048	2.83
Ca(CO)3	0.0048	2.83
CoF3	0.0014	0.85
NiO*OH	0.0048	2.83
H2FeAl(PO4)6(OH)8*16(H2O)	0.0048	2.83
Ca(OH)2	0.0048	2.83
Total	**0.1686**	**1**
(Ammonia) Mixed Hydroxide Precipitation Output		
Filtrate	**kg**	**wt%**
C	4.05E-05	3
CaCO3	0.0012	89
NaMnFeO2	0.000108	8
Total	**0.00135**	**100**

Table 13. ICP-OES Analysis of Lithium Salt Conducted by IME Fraunhofer.

Element	wt%
Al	
B	0.048
Ca	60.762
Co	0.010
Cu	0.005
Fe	0.047
Li	38.513
Mg	0.008
Mn	0.016
Na	0.285
Ni	0.063
P	
S	0.179
Si	0.066

5. Results

5.1. Recyclability Index and Ecolabeling of Products

The incorporation of a Recycling Index stands out as a crucial metric in assessing the effectiveness of recycling efforts, encompassing both products and the materials they contain. This index is derived by calculating the recovery rate of individual elements relative to their total weight, providing a detailed evaluation of their sustainability impact. This underscores the importance of adopting a product-centric approach to recycling.

As demonstrated in Table 14, comprehensive elemental weights of the Battery cell NMC811 were meticulously evaluated both before and after undergoing the recycling process. This assessment allowed for the determination of recovery rates. In accordance with proposals by [1], and as shown in Figure 5, leveraging this data could enable the development of a product label that effectively communicates its recycling efficiency or inefficiency. Such labeling not only enhances consumer awareness but also promotes sustainable practices across the lifecycle of products.

Table 14. Recyclability index from a product perspective showing the overall recovery rate of all elements within the NMC811 battery cell.

Element	Weight in Batery Cell (kg)	Recovery weight	Recovery Rate
Cu	0.07	0.013	19.24
C	0.396	0.228	57.49
Al	0.05	0	0
Li	0.026	0.016	59.79
Ni	0.2	0.194	97.34
Mn	0.02	0.018	89.61
Co	0.021	0.021	98.03
Fe	0.056	0.038	68.3
P	0.006	0	0
F	0.04	0	0
Total	**0.888**	**0.528**	**59.468**

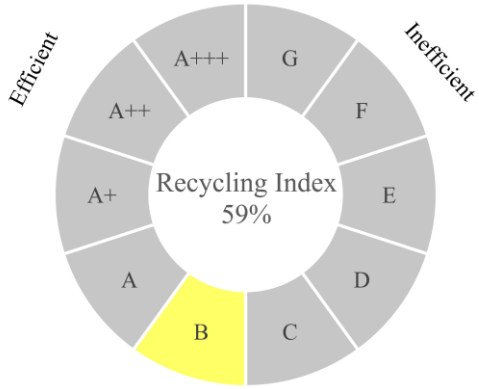

Figure 5. Recycling Efficiency Label for NMC 811 Battery Cell.

5.2. Results based on rules and guidelines

a) **Product-specific and recycling system-specific:** The designated recycling route, integrating mechanical, physical, and chemical processes, has been meticulously customized for the NMC811 battery cell, thereby establishing a distinctive recyclability profile. This approach encompasses the efficient recovery of lithium salt as a final product, while also prioritizing the extraction of other valuable materials as intermediate products.
b) **Model and simulation quantification:** The material and substance flow analysis was developed using HSC Sim, while the equilibrium mode for pyrolysis was done using FactSage. The integration and computation of this information enable us to establish a robust simulation model.
c) **Data in a consistent format:** The generated data has been meticulously presented in both weight (wt) and weight percentage (wt%) formats to facilitate clear comprehension of material flow dynamics. This approach ensures that stakeholders involved in the DfR process for the NMC811 battery cell can easily access and utilize the information. By integrating these detailed metrics, the material flow throughout the recycling process becomes transparent, allowing for informed decision-making and optimization of recycling strategies.
d) **Identify and minimize the use of materials that will cause losses and contamination:** As illustrated in Figure 6, the Metal Wheel diagram proposed by [2] serves as a comprehensive tool for assessing the expected losses in various recovery routes tailored for NMC811 battery cells. This diagram not only highlights the potential losses associated with each recovery pathway but also emphasizes the importance of selecting appropriate routes to mitigate these losses effectively. In this context, when choosing a specific recovery route, it is anticipated that there will be inherent losses. This study, therefore, underscores the significance of avoiding the combination of incompatible materials during the recycling process. By integrating these considerations, stakeholders can make informed decisions aimed at optimizing recovery efficiency while minimizing resource wastage and environmental impact.

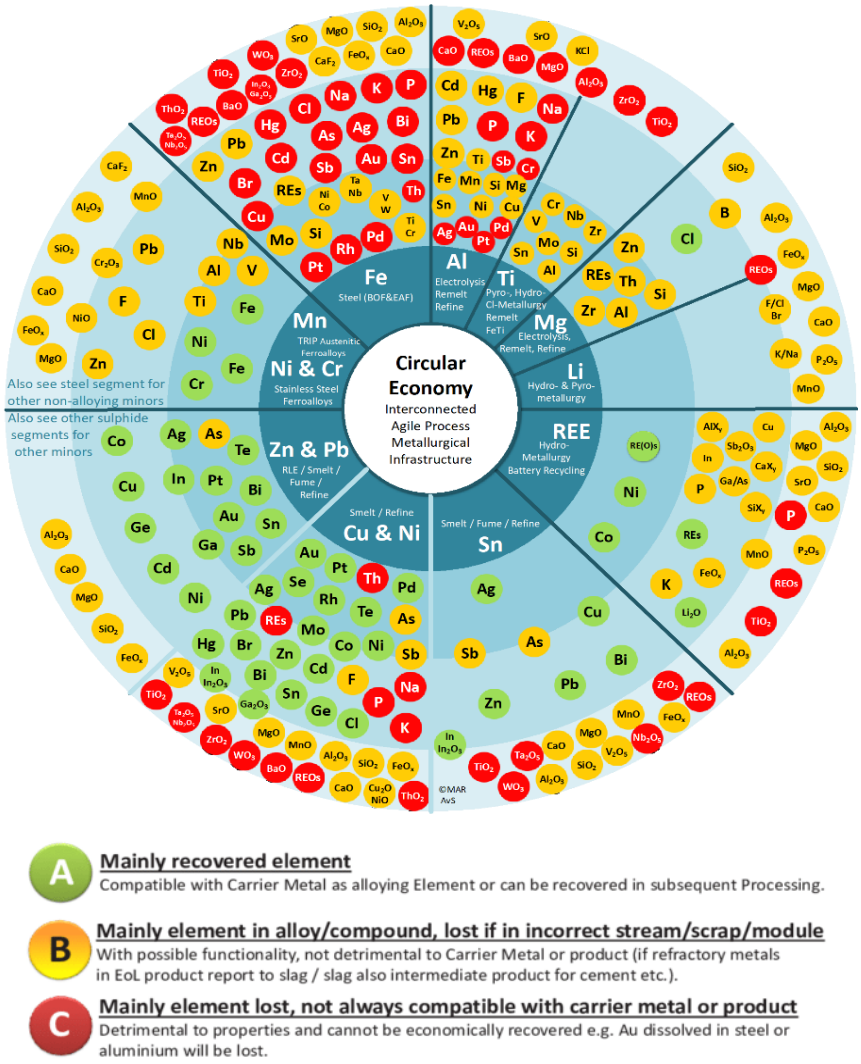

Figure 6. The losses observed in the chosen metallurgical recovery route are consistent with the metallurgical wheel, indicating that different materials are incompatible when processed together. Nevertheless, it doesn't indicate process efficiency.

e) **Design cluster or subunits in products that can be easily removed and that match with the final treatment:** Unifying parts or designing clusters for processing can significantly enhance recovery rates by reducing contamination within the process. However, this approach necessitates achieving a high liberation rate. Processing the anode and cathode together is expected to result in inevitable losses. This strategy underscores the importance of targeted material recovery to improve overall efficiency and reduce waste in the recycling process.

f) **Label:** A recycling label has been developed to indicate the total recovery of materials after the recycling process. This label provides a clear indication of the product's efficiency or inefficiency in terms of recyclability. By showcasing the effectiveness of the recycling process, the label serves as a valuable tool for assessing the sustainability and environmental impact of the product.

5.3. Life cycle assessment considering DfR approach

Table 15 summarizes the environmental impacts of various processing stages in terms of Global Warming Potential (GWP), Acidification, Human Toxicity, and Eutrophication. The units used are kilograms of CO2 equivalents (kg CO2-eq) for GWP, kilograms of SO2 equivalents (kg SO2-eq) for Acidification, kilograms of 1,4-dichlorobenzene equivalents (kg 1,4-DCB-eq) for Human Toxicity, and kilograms of phosphate equivalents (kg PO4-eq) for Eutrophication. This comprehensive analysis provides a clear depiction of the environmental impacts associated with each processing stage, enabling targeted efforts to optimize sustainability and minimize ecological footprint.

Table 15. LCA results obtained from IME Fraunhofer.

	GWP kg CO2-eq	Acidification kg SO2-eq	Human Toxicity kg 1,4-DCB-eq	Eutrophication kg PO4-eq
Laser Cut	8.76E-03	1.93E-05	1.96E-12	1.31E-05
EHZ	7.27E-01	2.37E-03	1.93E-10	9.58E-04
SuSi	1.30	2.12E-03	6.83E-10	6.56E-04
Pyrolysis	5.85	1.57E-02	1.43E-09	8.21E-03
Leaching	4.27E-01	1.25E-03	1.06E-10	1.26E-04
Precipitation	1.65	5.70E-03	3.16E-10	6.31E-04
Total	**9.97**	**2.72E-02**	**2.73E-09**	**1.06E-02**

In Figure 7, a DfR approach has been implemented. The strategy entails designing the battery cell with a casing that is easily dismountable, thereby facilitating the direct transfer of the anode, cathode, separator foil, and electrolyte to a pyrolysis process unit. This design modification is projected to yield substantial environmental benefits, including a 20% reduction in Global Warming Potential (GWP), a 16% reduction in Acidification, a 32% reduction in Human Toxicity, and a 15% reduction in Eutrophication impacts. These reductions highlight the significant potential of DfR principles in mitigating the environmental footprint of battery recycling processes.

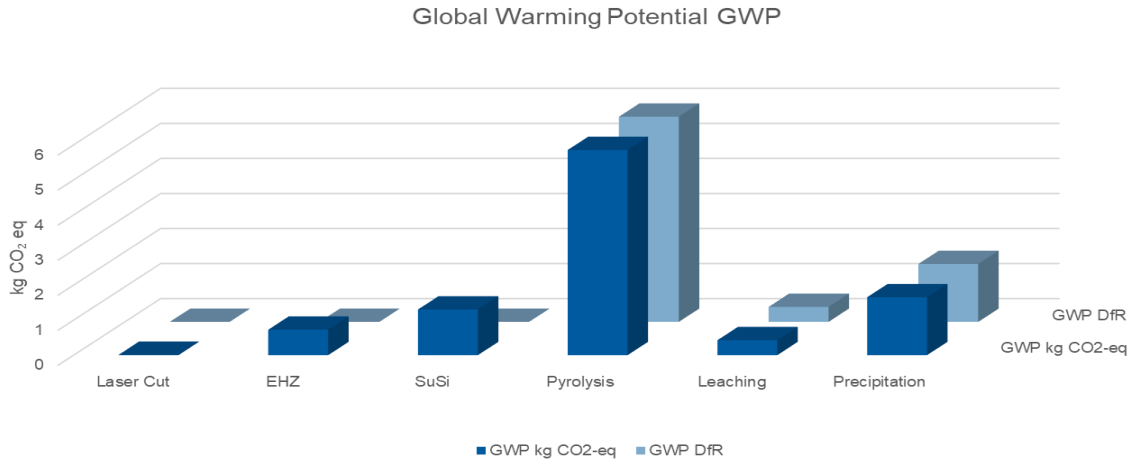

Figure 7. Environmental Benefits of DfR Approach for NMC811 Battery Cells.

Additionally, Figure 8 shows a second DfR approach where the battery cell is designed with an easily removable casing and employs a binder and electrolyte free of fluorine, thereby eliminating the need for a defluorination unit after leaching, we can achieve further significant environmental benefits. These enhancements would result in a 21% reduction in Global Warming Potential (GWP), a 17% reduction in Acidification, a 32% reduction in Human Toxicity, and a 15% reduction in Eutrophication impacts. This demonstrates the substantial environmental advantages of incorporating fluorine-free components and easily dismountable casings in battery cell design.

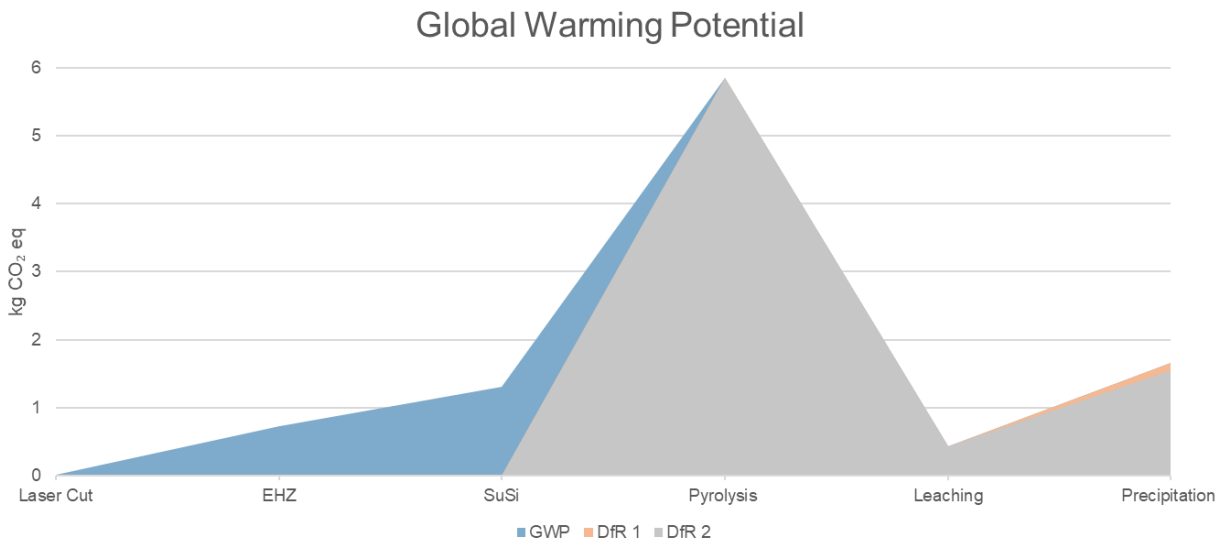

Figure 8. Environmental Benefits of second DfR Approach for NMC811 Battery Cells.

6. Conclusions:

The Anode and Cathode: Designing the battery cell with an easily dismountable casing allows for the direct processing of the anode, cathode, separator foil, and electrolyte in a pyrolysis unit, yielding significant environmental benefits. This design modification results in a 20% reduction in Global Warming Potential (GWP), a 16% reduction in Acidification, a 32% reduction in Human Toxicity, and a 15% reduction in Eutrophication impact categories. Such a design facilitates more efficient and environmentally friendly recycling processes by enabling easier access to critical components.

The Binder: Traditional binders like polyvinylidene fluoride (PVDF) are soluble in a limited range of solvents, which can complicate the recycling process. Alternative binders that can disperse in water, such as carboxymethyl cellulose (CMC) or styrene–butadiene rubber (SBR), present distinct advantages. PVDF's mechanical properties, such as hardness and modulus of elasticity, deteriorate with age, negatively impacting the electrode's adhesiveness to the active material. Exploring binders that do not

require solvents or even electrodes that forgo binders altogether could enhance recycling efficiency and material recovery.

The Electrolyte: Fluorine-containing components in used batteries introduce additional processing complexities. Incorporating a fluoride precipitation unit necessitates the use of more reagents, complicating the recycling process. Therefore, the defluorination of lithium-ion batteries is highly beneficial. Implementing this approach results in a 21% reduction in GWP, a 17% reduction in Acidification, a 32% reduction in Human Toxicity, and a 15% reduction in Eutrophication, thereby significantly improving the environmental footprint of the recycling process.

Delamination: Separating the anode and cathode during recycling can prevent copper (Cu) and aluminum (Al) from becoming contaminants in hydrometallurgical processes. For example, aluminum foils are susceptible to oxidation and corrosion, which can introduce impurities during a froth flotation process used for active particle separation. Including a delamination process unit before physical and chemical processing can enhance the recycling index from 59% to 71%, ensuring cleaner and more efficient material recovery.

Before Dismantling: Proper discharge procedures are crucial to avoid undesirable side reactions, such as anode dissolution into the electrolyte and the formation of copper dendrites, which can contaminate material streams, including the cathode. Low-voltage cells should be discharged using a salt solution like NaCl or KCl to mitigate these issues, thereby ensuring the integrity of the recycling process.

Before Leaching: Incorporating a froth flotation process for active particle separation after implementing these recommendations can significantly enhance material recovery [3] . This process facilitates the separation of carbon (C) from the black mass, increasing the recovery of anode material and boosting the recycling index to 90%. In this scenario, it is crucial to use an alternative binder type, as the binder used in the anode can reharden after pyrolysis, leading to the formation of non-selective agglomerates. This consideration is essential for optimizing the recycling process and ensuring the highest possible material recovery rates.

Bibliography

1. Reuter, M.A. and A. van Schaik, *Material and product-centric recycling: design for recycling rules and digital methods*, in *Handbook of Recycling*. 2024, Elsevier. p. 79-95.
2. Reuter, M.A. and I.V. Kojo, *Challenges of metal recycling.* Materia, 2012. **2**(2012): p. 50-57.
3. Vanderbruggen, A., et al., *Lithium-ion battery recycling– influence of recycling processes on component liberation and flotation separation efficiency.* ACS ES&T Engineering, 2022. **2**(11): p. 2130-2141.